

# Electric dipole moments of neutron and heavy quarks in the B-LSSM

Jin-Lei Yang<sup>1,2,3\*</sup>, Tai-Fu Feng<sup>1,2,4†</sup>, Sheng-Kai

Cui<sup>1,2</sup>, Chang-xin Liu<sup>1,2</sup>, Wei Li<sup>1,2</sup>, Hai-Bin Zhang<sup>1,2‡</sup>

*Department of Physics, Hebei University, Baoding, 071002, China<sup>1</sup>*

*Hebei Key Lab of High-precision Computation and Application*

*of Quantum Field Theory, Baoding, 071002, China<sup>2</sup>*

*CAS Key Laboratory of Theoretical Physics, School of Physical Sciences,*

*University of Chinese Academy of Sciences, Beijing 100049, China<sup>3</sup>*

*Department of Physics, Chongqing University, Chongqing 401331, China<sup>4</sup>*

## Abstract

The searching for the electric dipole moments (EDMs) of neutron ( $d_n$ ),  $b$  quark ( $d_b$ ) and  $c$  quark ( $d_c$ ) gives strict upper bounds on these quantities. And recently, new upper bounds on  $d_b$ ,  $d_c$  are obtained by the strict limit on  $d_n$ . The models of new physics (NP) with additional CP-violating (CPV) sources are constrained strictly by these EDMs. In this work, we focus on the CPV effects on these EDMs in the minimal supersymmetric extension (MSSM) of the SM with local  $B-L$  gauge symmetry (B-LSSM). The contributions from one-loop and some two-loop diagrams to the quark EDM are given in general form, which can also be used in the calculation of quark EDM in other models of NP. Considering the constrains from updated experimental data, the numerical results show that the two-loop corrections can make important contributions to these EDMs. Compared with the MSSM, the effects of new CPV phases and new parameters in the B-LSSM on these EDMs are also explored.

PACS numbers:

Keywords: quark, neutron, EDM, B-LSSM

---

\* yangjinlei@itp.ac.cn

† fengtf@hbu.edu.cn

‡ hbzhang@hbu.edu.cn

## I. INTRODUCTION

In the standard model (SM), the only sources of CP-violating (CPV) are the Cabbibo-Kobayashi-Maskawa (CKM) phases, which appears to be the origin of the CPV phenomena observed in nondiagonal processes involving the  $K$  and  $B$  mesons [1–3]. However, the observed baryon asymmetry of the universe indicates that, the CPV sources in the SM are not sufficient, and new CPV sources are needed to generate the observed baryon asymmetry. In addition, it is well known that, the theoretical predictions on electric dipole moments (EDMs) in the SM are too tiny to be detected in near future. When new CPV phases are introduced, the theoretical predications on EDMs can be enhanced vastly, hence the EDM of elementary particle is a clear signal of CPV [4–8]. As a result, studying the EDMs of elementary particles is of prime importance, and measurements on the EDMs of neutron or fundamental particles provide sensitive approaches to investigate potential new sources of CPV. So far no EDM for the neutron,  $b$  quark or  $c$  quark has been detected, but strong bounds on these quantities have been obtained [9–13]

$$\begin{aligned}
 |d_n| &< 3.0 \times 10^{-26} \text{e} \cdot \text{cm}, \\
 |d_b| &< 2.0 \times 10^{-17} \text{e} \cdot \text{cm}, \\
 |d_c| &< 4.4 \times 10^{-17} \text{e} \cdot \text{cm}.
 \end{aligned}
 \tag{1}$$

In addition, the chromo-EDM (CEDM) of heavy quark is constrained by the strict limit on the neutron EDM. The EDM of neutron can be expressed in terms of fundamental dipoles [14]

$$d_n = (1 \pm 0.5)[1.4(d_d^\gamma - 0.25d_u^\gamma) + 1.1e(d_d^g + 0.5d_u^g)] \pm (22 \pm 10) \text{MeV}C_5,
 \tag{2}$$

where  $d_q^\gamma$ ,  $d_q^g$ ,  $C_5$  denote the quark EDM of  $q$  from the electroweak interaction, the CEDM of  $q$  and the coefficient of Weinberg operator at the chirality scale, respectively. Using the running from Refs. [15, 16] at one-loop,  $d_{d,u}^{\gamma,g}$  and  $C_5$  can be expressed in terms of  $d_c^g$  at the scale  $m_c$  [13]. Combining with the limits on  $d_n$ , new upper limit on  $d_c^g$  is obtained [13],  $|d_c^g| < 1.0 \times 10^{-22} \text{cm}$ . Then, assuming constructive interference between the EDM and

CEDM contributions at the NP scale [17], new bounds on the EDM of  $b$  and  $c$  quark are derived by using the stringent limits on  $d_b^g$  in Ref. [18] and  $d_c^g$  in Ref. [13]

$$\begin{aligned} |d_b| &< 1.2 \times 10^{-20} \text{e} \cdot \text{cm}, \\ |d_c| &< 1.5 \times 10^{-21} \text{e} \cdot \text{cm}, \end{aligned} \tag{3}$$

which improves the previous ones in Eq. (1) by about three orders of magnitude. Since the experimental upper bounds on these quantities are very small, the contributions from new CPV phases are limited strictly by the present experimental data, hence researching NP effects on these EDMs may shed light on the mechanism of CPV.

In extensions of the SM, the supersymmetry is considered as one of the most plausible candidates. For the explanation of baryon asymmetry, electroweak baryogenesis (EWB) is one of the most well-known mechanisms, and new CPV phases are needed to enhance the asymmetry in this case. In Refs. [19–23], EWB is discussed in the MSSM in great detail, and the results show that the  $\mu$  term (the bilinear Higgs mass term in the superpotential) is the dominate source of baryon asymmetry. However, when the phase of  $\mu$  is taken to be large, the theoretical predictions of the EDMs are larger than corresponding upper bounds by several orders of magnitude. The effects have been explored in Refs. [24–32]. The results show that, the most interesting possibility to suppress these EDMs to below the corresponding experimental upper bounds is, the contributions from different phases cancel each other. The CPV characters in supersymmetry are very interesting and studies on them may shed some light on the general characteristics of the supersymmetric model.

In this work, we explore the CPV effects on the EDM of neutron  $d_n$ ,  $b$  quark  $d_b$  and  $c$  quark  $d_c$  in the MSSM with local  $B - L$  gauge symmetry (B-LSSM) [33–36]. The model is based on the gauge symmetry group  $SU(3) \otimes SU(2)_L \otimes U(1)_Y \otimes U(1)_{B-L}$ , where  $B$  stands for the baryon number and  $L$  stand for the lepton number respectively. Compared with the MSSM, there are much more candidates for the dark matter [37–40] in the B-LSSM, which also accounts elegantly for the existence and smallness of the left-handed neutrino masses. Since the exotic singlet Higgs and right-handed (s) neutrinos [41–46] releases additional parameter space from the LHC constraints, the model alleviates the little hierarchy problem of the MSSM [47]. In addition, the invariance under  $U(1)_{B-L}$  gauge group imposes the

R-parity conservation, which is assumed in the MSSM to avoid proton decay. And R-parity conservation can be maintained if  $U(1)_{B-L}$  symmetry is broken spontaneously [48].

The paper is organized as follows. In Sec. II, the main ingredients of the B-LSSM are summarized briefly by introducing the superpotential and the general soft breaking terms. Then the analysis on the EDM of neutron  $d_n$ ,  $b$  quark  $d_b$  and  $c$  quark  $d_c$  are presented in Sec. III. In order to see the corrections to these EDMs clearly, the numerical results of  $d_n$ ,  $d_b$ ,  $d_c$  with new CPV phases are explored in Sec. IV. Conclusions are summarized in Sec. V.

## II. THE B-LSSM

Besides the superfields of the MSSM, two chiral singlet superfields  $\hat{\eta}_1 \sim (1, 1, 0, -1)$ ,  $\hat{\eta}_2 \sim (1, 1, 0, 1)$  and three generations of right-handed neutrinos are introduced in the B-LSSM. And the local gauge group is enlarged to  $SU(3)_C \otimes SU(2)_L \otimes U(1)_Y \otimes U(1)_{B-L}$  in the model, where the  $U(1)_{B-L}$  is spontaneously broken by the chiral singlets. This version of B-LSSM is encoded in SARAH [49], which is used to create the mass matrices and interaction vertexes in the model. Then the local gauge symmetry  $SU(2)_L \otimes U(1)_Y \otimes U(1)_{B-L}$  breaks down to the electromagnetic symmetry  $U(1)_{em}$  as the Higgs fields receive vacuum expectation values:

$$\begin{aligned} H_1^1 &= \frac{1}{\sqrt{2}}(v_1 + \text{Re}H_1^1 + i\text{Im}H_1^1), & H_2^2 &= \frac{1}{\sqrt{2}}(v_2 + \text{Re}H_2^2 + i\text{Im}H_2^2), \\ \tilde{\eta}_1 &= \frac{1}{\sqrt{2}}(u_1 + \text{Re}\tilde{\eta}_1 + i\text{Im}\tilde{\eta}_1), & \tilde{\eta}_2 &= \frac{1}{\sqrt{2}}(u_2 + i\text{Re}\tilde{\eta}_2 + i\text{Im}\tilde{\eta}_2). \end{aligned} \quad (4)$$

Then in analogy to the ratio of the MSSM VEVs ( $\tan\beta = \frac{v_2}{v_1}$ ), we can define  $\tan\beta' = \frac{u_2}{u_1}$ .

In addition, the superpotential of the B-LSSM can be written as

$$\begin{aligned} W &= Y_u^{ij} \hat{Q}_i \hat{H}_2 \hat{U}_j^c + \mu \hat{H}_1 \hat{H}_2 - Y_d^{ij} \hat{Q}_i \hat{H}_1 \hat{D}_j^c - Y_e^{ij} \hat{L}_i \hat{H}_1 \hat{E}_j^c + \\ &Y_{\nu,ij} \hat{L}_i \hat{H}_2 \hat{\nu}_j^c - \mu' \hat{\eta}_1 \hat{\eta}_2 + Y_{x,ij} \hat{\nu}_i^c \hat{\eta}_1 \hat{\nu}_j^c, \end{aligned} \quad (5)$$

where  $i, j$  are generation indices. Correspondingly, the soft breaking terms of the B-LSSM are generally given as

$$\mathcal{L}_{soft} = \left[ -\frac{1}{2}(M_1 \tilde{\lambda}_B \tilde{\lambda}_B + M_2 \tilde{\lambda}_W \tilde{\lambda}_W + M_3 \tilde{\lambda}_g \tilde{\lambda}_g + 2M_{BB'} \tilde{\lambda}_{B'} \tilde{\lambda}_B + M_{B'} \tilde{\lambda}_{B'} \tilde{\lambda}_{B'}) - \right.$$

$$\begin{aligned}
& B_\mu H_1 H_2 - B_{\mu'} \tilde{\eta}_1 \tilde{\eta}_2 + T_{u,ij} \tilde{Q}_i \tilde{u}_j^c H_2 + T_{d,ij} \tilde{Q}_i \tilde{d}_j^c H_1 + T_{e,ij} \tilde{L}_i \tilde{e}_j^c H_1 + T_\nu^{ij} H_2 \tilde{\nu}_i^c \tilde{L}_j + \\
& T_x^{ij} \tilde{\eta}_1 \tilde{\nu}_i^c \tilde{\nu}_j^c + h.c. ] - m_{\tilde{\nu},ij}^2 (\tilde{\nu}_i^c)^* \tilde{\nu}_j^c - m_{\tilde{q},ij}^2 \tilde{Q}_i^* \tilde{Q}_j - m_{\tilde{u},ij}^2 (\tilde{u}_i^c)^* \tilde{u}_j^c - m_{\tilde{\eta}_1}^2 |\tilde{\eta}_1|^2 - \\
& m_{\tilde{\eta}_2}^2 |\tilde{\eta}_2|^2 - m_{\tilde{d},ij}^2 (\tilde{d}_i^c)^* \tilde{d}_j^c - m_{\tilde{L},ij}^2 \tilde{L}_i^* \tilde{L}_j - m_{\tilde{e},ij}^2 (\tilde{e}_i^c)^* \tilde{e}_j^c - m_{H_1}^2 |H_1|^2 - m_{H_2}^2 |H_2|^2, \quad (6)
\end{aligned}$$

where  $\tilde{\lambda}_B, \tilde{\lambda}_{B'}$  denote the gauginos of  $U(1)_Y$  and  $U(1)_{(B-L)}$  respectively.

It can be noted that there are two Abelian groups in the B-LSSM, which gives rise to a new effect absent in the MSSM or other SUSY models with just one Abelian gauge group: the gauge kinetic mixing. This mixing couples the  $B-L$  sector to the MSSM sector, and it can be induced through RGEs [50–56] even if it is set to zero at  $M_{GUT}$ . Immediate interesting consequences of the gauge kinetic mixing arise in various sectors of the model. Firstly, the gauge kinetic mixing leads to the mixing between the  $H_1^1, H_2^2, \tilde{\eta}_1, \tilde{\eta}_2$  at the tree level, which changes the vacuum structure vastly and also affects the theoretical prediction on the SM-like Higgs boson mass. Meanwhile,  $\tilde{\lambda}_{B'}$  mixes with the two higgsinos in the MSSM at the tree level. Then new gauge boson  $Z'$  mixes with the  $Z$  boson in the MSSM, and new gauge coupling constant  $g_{YB}$  is introduced. In addition, additional D-terms contribute to the mass matrices of the squarks and sleptons, which affects the theoretical predictions on various observations of the model. All of these properties of the model are introduced in detail in our earlier work [57, 58].

### III. THE EDMS OF NEUTRON AND HEAVY QUARKS

For the neutron EMD  $d_n$ , we adopt the values 0.5 and 12 MeV for the coefficients  $1 \pm 0.5$  and  $22 \pm 10$  MeV in Eq. (2) respectively, in order to coincide with the discussion in Ref. [13]. In addition, at the low scale, the quark EDM can be written as

$$d_q = d_q^{\gamma}(\Lambda_\chi) + \frac{e}{4\pi} d_q^g(\Lambda_\chi) + \frac{e\Lambda_\chi}{4\pi} C_5(\Lambda_\chi), \quad (7)$$

where  $\Lambda_\chi = m_q$  denotes the chirality breaking scale,  $m_q$  denotes the corresponding quark mass. The Wilson coefficient of the purely gluonic Weinberg operator originates from the two-loop "gluino-squark" diagrams, and the concrete expression of  $C_5$  can be written as [59–

61]

$$C_5(\Lambda) = -\frac{3g_3^5}{(4\pi)^4 M_3^3} \left\{ m_t \Im[e^{2i\theta_3} (Z_{\tilde{t}})_{2,2} (Z_{\tilde{t}})_{2,1}^\dagger] \frac{x_{\tilde{t}_1} - x_{\tilde{t}_2}}{x_{M_3}} H\left(\frac{x_{\tilde{t}_1}}{x_{M_3}}, \frac{x_{\tilde{t}_2}}{x_{M_3}}, \frac{x_t}{x_{M_3}}\right) \right. \\ \left. + m_b \Im[e^{2i\theta_3} (Z_{\tilde{b}})_{2,2} (Z_{\tilde{b}})_{2,1}^\dagger] \frac{x_{\tilde{b}_1} - x_{\tilde{b}_2}}{x_{M_3}} H\left(\frac{x_{\tilde{b}_1}}{x_{M_3}}, \frac{x_{\tilde{b}_2}}{x_{M_3}}, \frac{x_b}{x_{M_3}}\right) \right\}, \quad (8)$$

where  $\Lambda$  denotes the matching scale,  $Z_{\tilde{t}}(Z_{\tilde{b}})$  is the diagonalizing matrix for the squared mass matrix of stop (sbottom), and the function  $H$  can be found in Refs. [59–61].

Meanwhile,  $d_q^\gamma$ ,  $d_q^g$  and  $C_5$  are evolved with the renormalization group equations from the matching scale  $\Lambda$  down to the chirality breaking scale  $\Lambda_\chi$  [62] according to

$$d_q^\gamma(\Lambda_\chi) = 1.53d_q^\gamma(\Lambda), \quad d_q^g(\Lambda_\chi) = 3.4d_q^g(\Lambda), \quad C_5(\Lambda_\chi) = 3.4C_5(\Lambda). \quad (9)$$

The effective Lagrangian for the quark EDMs can be written as

$$\mathcal{L}_{EDM} = -\frac{i}{2} d_q^\gamma \bar{q} \sigma^{\mu\nu} \gamma_5 q F_{\mu\nu}, \quad (10)$$

where  $\sigma^{\mu\nu} = i[\gamma^\mu, \gamma^\nu]/2$ ,  $q$  is the wave function for quark, and  $F_{\mu\nu}$  is the electromagnetic field strength. Adopting the effective Lagrangian approach, the quark EDMs can be written as

$$d_q^\gamma = -\frac{2eQ_q m_q}{(4\pi)^2} \Im(C_2^R + C_2^{L*} + C_6^R), \quad (11)$$

where  $C_{2,6}^{L,R}$  represent the Wilson coefficients of the corresponding operators  $O_{2,6}^{L,R}$

$$O_2^{L,R} = \frac{eQ_q}{(4\pi)^2} (-iD_\alpha^*) \bar{q} \gamma^\alpha F \cdot \sigma P_{L,R} q, \\ O_6^{L,R} = \frac{eQ_q m_q}{(4\pi)^2} \bar{q} F \cdot \sigma P_{L,R} q, \quad (12)$$

Similarly, the effective Lagrangian for the quark CEDMs can be written as

$$\mathcal{L}_{CEDM} = -\frac{i}{2} d_q^g \bar{q} \sigma^{\mu\nu} \gamma_5 q G_{\mu\nu}^a T^a, \quad (13)$$

where  $G_{\mu\nu}$  is the  $SU(3)$  gauge field strength,  $T^a$  is the  $SU(3)$  generators. Then the quark CEDMs can be written as

$$d_q^g = -\frac{2g_3 m_q}{(4\pi)^2} \Im(C_7^R + C_7^{L*} + C_8^R), \quad (14)$$

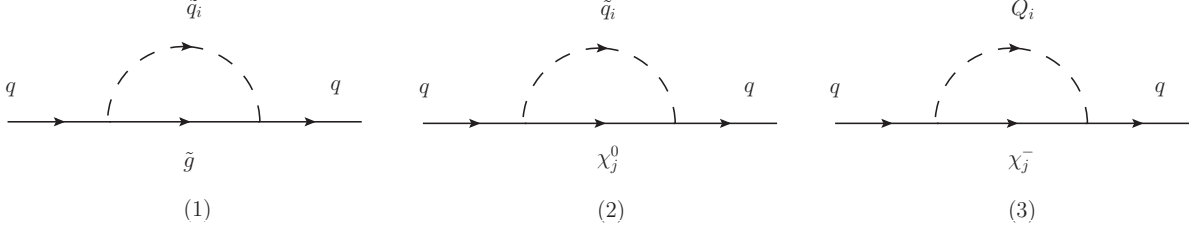


FIG. 1: The one-loop diagrams which contributes to  $d_q^\gamma$  and  $d_q^g$  are obtained by attaching a photon and a gluon respectively to the internal particles in all possible ways.

where  $C_{7,8}^{L,R}$  represent the Wilson coefficients of the corresponding operators  $O_{7,8}^{L,R}$

$$\begin{aligned} O_7^{L,R} &= \frac{g_3}{(4\pi)^2} (-iD_\alpha^*) \bar{q} \gamma^\alpha G^a \cdot \sigma T^a P_{L,R} q, \\ O_8^{L,R} &= \frac{g_3 m_q}{(4\pi)^2} \bar{q} G^a \cdot \sigma T^a P_{L,R} q, \end{aligned} \quad (15)$$

The one-loop Feynman diagrams contributing to the above amplitudes are depicted in Fig. 1. Calculating the Feynman diagrams,  $d_q^\gamma$  and  $d_q^g$  at the one-loop level can be written as

$$\begin{aligned} d_q^{\gamma(1)} &= \frac{e_q e}{12\pi^2 m_W} \frac{\sqrt{x_{\tilde{g}}}}{x_{\tilde{q}_i}} \Im [C_{\tilde{g}\tilde{q}_i q}^L C_{\tilde{q}\tilde{q}_i \tilde{g}}^L] I_1\left(\frac{x_{\tilde{g}}}{x_{\tilde{q}_i}}\right), \\ d_q^{g(1)} &= \frac{-g_3}{32\pi^2 m_W} \frac{\sqrt{x_{\tilde{g}}}}{x_{\tilde{q}_i}} \Im [C_{\tilde{g}\tilde{q}_i q}^L C_{\tilde{q}\tilde{q}_i \tilde{g}}^L] I_2\left(\frac{x_{\tilde{g}}}{x_{\tilde{q}_i}}\right), \\ d_q^{\gamma(2)} &= \frac{e_q e}{32\pi^2 m_W} \frac{\sqrt{x_{\chi_j^0}}}{x_{\tilde{q}_i}} \Im [C_{\tilde{q}\tilde{q}_i \chi_j^0}^L C_{\tilde{\chi}_j^0 \tilde{q}_i q}^R] I_1\left(\frac{x_{\chi_j^0}}{x_{\tilde{q}_i}}\right), \\ d_q^{g(2)} &= \frac{g_3^3}{128\pi^2 e^2 m_W} \frac{\sqrt{x_{\chi_j^0}}}{x_{\tilde{q}_i}} \Im [C_{\tilde{q}\tilde{q}_i \chi_j^0}^L C_{\tilde{\chi}_j^0 \tilde{q}_i q}^R] I_1\left(\frac{x_{\chi_j^0}}{x_{\tilde{q}_i}}\right), \\ d_q^{\gamma(3)} &= \frac{e}{16\pi^2 m_W} \frac{\sqrt{x_{\chi_j^-}}}{x_{\tilde{Q}_i}} \Im [C_{\tilde{q}\tilde{Q}_i \chi_j^-}^L C_{\tilde{\chi}_j^- \tilde{Q}_i q}^R] \left[ e_Q I_1\left(\frac{x_{\chi_j^-}}{x_{\tilde{Q}_i}}\right) + (e_q - e_Q) I_3\left(\frac{x_{\chi_j^-}}{x_{\tilde{q}_i}}\right) \right], \\ d_q^{g(3)} &= \frac{g_3^3}{16\pi^2 e^2 m_W} \frac{\sqrt{x_{\chi_j^-}}}{x_{\tilde{Q}_i}} \Im [C_{\tilde{q}\tilde{Q}_i \chi_j^-}^L C_{\tilde{\chi}_j^- \tilde{Q}_i q}^R] I_1\left(\frac{x_{\chi_j^-}}{x_{\tilde{Q}_i}}\right), \end{aligned} \quad (16)$$

where  $x_i$  denotes  $m_i^2/m_W^2$ ,  $g_3$  is the strong coupling constant,  $C_{abc}^{L,R}$  denotes the constant parts of the interaction vertex about  $abc$ , which can be got through SARAH, and  $a, b, c$  denote the interacting particles. The functions  $I_{1,2,3}$  can be written as

$$I_1(x) = \frac{1}{2(x-1)^2} \left( 1 + x + \frac{2x}{x-1} \ln x \right), \quad (17)$$

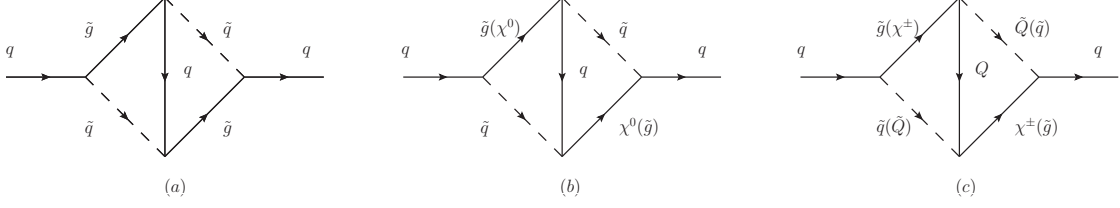


FIG. 2: The two-loop diagrams which contributes to  $d_q^\gamma$  and  $d_q^g$  are obtained by attaching a photon and a gluon respectively to the internal particles in all possible ways.

$$I_2(x) = \frac{1}{6(x-1)^2} \left( 10x - 26 - \frac{2x-18}{x-1} \ln x \right), \quad (18)$$

$$I_3(x) = \frac{1}{2(x-1)^2} \left( 3 - x + \frac{2}{x-1} \ln x \right). \quad (19)$$

The two-loop gluino corrections to the Wilson coefficients from the self-energy diagrams for quarks are considered, the corresponding Feynman diagrams are depicted in Fig. 2. The corresponding dipole moment diagrams are obtained by attaching a photon or gluon to the internal particles in all possible ways. Then, the contributions from these two-loop diagrams to  $d_q^\gamma$  and  $d_q^g$  can be written as

$$\begin{aligned}
d_q^{\gamma(a)} &= \frac{-4e_q e g_3^2 |m_{\tilde{g}}|}{9(4\pi)^4 m_W^2} F_3(x_q, x_{\tilde{q}_j}, x_{\tilde{g}}, x_{\tilde{g}}, x_{\tilde{q}_i}) \Im [C_{\tilde{q}\tilde{g}\tilde{q}_j}^L C_{\tilde{g}\tilde{q}\tilde{q}_j}^L], \\
d_q^{g(a)} &= d_q^{\gamma(a)} g_3 / (e_q e), \\
d_q^{\gamma(b)} &= \frac{4e_q e}{3(4\pi)^4 m_W^2} \left\{ |m_{\tilde{g}}| F_4(x_q, x_{\tilde{q}_j}, x_{\tilde{g}}, x_{\chi_k^0}, x_{\tilde{q}_i}) \Im [C_{\tilde{\chi}_k^0 q \tilde{q}_j}^R C_{\tilde{\chi}_k^0 q \tilde{q}_i}^L C_{\tilde{g}\tilde{q}\tilde{q}_j}^L C_{\tilde{g}\tilde{q}\tilde{q}_i}^L - C_{\tilde{\chi}_k^0 q \tilde{q}_j}^L \right. \\
&\quad \times C_{\tilde{\chi}_k^0 q \tilde{q}_i}^R C_{\tilde{q}\tilde{g}\tilde{q}_j}^{L*} C_{\tilde{q}\tilde{g}\tilde{q}_i}^{L*}] - m_{\chi_k^0} F_5(x_q, x_{\tilde{q}_j}, x_{\tilde{g}}, x_{\chi_k^0}, x_{\tilde{q}_i}) \Im [C_{\tilde{\chi}_k^0 q \tilde{q}_j}^R C_{\tilde{\chi}_k^0 q \tilde{q}_i}^R C_{\tilde{q}\tilde{g}\tilde{q}_j}^{L*} C_{\tilde{q}\tilde{g}\tilde{q}_i}^L \\
&\quad \left. - C_{\tilde{\chi}_k^0 q \tilde{q}_j}^L C_{\tilde{\chi}_k^0 q \tilde{q}_i}^L C_{\tilde{q}\tilde{g}\tilde{q}_j}^{L*} C_{\tilde{q}\tilde{g}\tilde{q}_i}^L] \right\}, \\
d_q^{g(b)} &= d_q^{\gamma(b)} g_3 / (e_q e), \\
d_q^{\gamma(c)} &= \frac{2e}{3(4\pi)^4 m_W^2} \left\{ |m_{\tilde{g}}| F_4(x_Q, x_{\tilde{Q}_j}, x_{\tilde{g}}, x_{\chi_k^\pm}, x_{\tilde{q}_i}) \Im [C_{\tilde{Q}\chi_k^\pm \tilde{q}_j}^L C_{\tilde{q}\chi_k^\pm \tilde{Q}_i}^R C_{\tilde{g}\tilde{Q}\tilde{Q}_j}^L C_{\tilde{g}\tilde{q}\tilde{q}_i}^L - C_{\tilde{Q}\chi_k^\pm \tilde{q}_j}^R \right. \\
&\quad \times C_{\tilde{q}\chi_k^\pm \tilde{Q}_i}^L C_{\tilde{Q}\tilde{g}\tilde{Q}_j}^{L*} C_{\tilde{q}\tilde{g}\tilde{q}_i}^{L*}] - m_{\chi_k^\pm} F_5(x_Q, x_{\tilde{Q}_j}, x_{\tilde{g}}, x_{\chi_k^\pm}, x_{\tilde{q}_i}) \Im [C_{\tilde{Q}\chi_k^\pm \tilde{q}_j}^L C_{\tilde{q}\chi_k^\pm \tilde{Q}_i}^L C_{\tilde{Q}\tilde{g}\tilde{Q}_j}^{L*} C_{\tilde{q}\tilde{g}\tilde{q}_i}^L \\
&\quad \left. - C_{\tilde{Q}\chi_k^\pm \tilde{q}_j}^R C_{\tilde{q}\chi_k^\pm \tilde{Q}_i}^R C_{\tilde{g}\tilde{Q}\tilde{Q}_j}^L C_{\tilde{q}\tilde{g}\tilde{q}_i}^{L*}] \right\}, \\
d_q^{g(c)} &= d_q^{\gamma(c)} g_3 / e, \quad (20)
\end{aligned}$$

where the concrete expressions for the functions  $F_{3,4,5}$  can be found in Ref. [63]. The similar expressions of two-loop gluino contributions can be found in Ref. [63]. We translate them

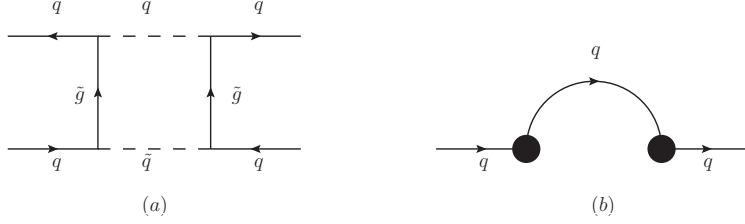


FIG. 3: Full theory diagram (a) and effective diagram (b) are plotted, where the blobs denote the effective vertexes, and a outgoing photon or gluon is attached by all possible ways.

into our notations, which is written in general form, and can be used in the calculation of quark EDM in other models of NP.

We should note that, there are infrared divergencies in Fig. 2 when the SM quarks appear as internal particles, because we calculate these diagrams by expanding the external momentum. In this case, matching full theory diagrams to the corresponding two-loop diagrams in Fig. 2 is needed to cancel the infrared divergency. Taking Fig. 2(a) as example to illustrate how to cancel the infrared divergency, the corresponding diagrams are shown in Fig. 3. When the external gluon is attached to an internal particle in Fig. 2(a), and the external gluon can be attached to the same internal particle in Fig. 3(a) or (b). Then infrared divergency in the diagram by attaching a gluon in Fig. 2(a) can be cancelled by subtracting the corresponding diagram by attaching a gluon in the same way in Fig. 3.

In addition, the two-loop Barr-Zee type diagrams can also make contributions to the quark EDM. The diagrams in which a closed fermion loop is attached to the virtual gauge bosons or Higgs fields are considered, and the corresponding Feynman diagrams are depicted in Fig. 4. Then, the contributions from these two-loop Barr-Zee type diagrams to  $d_q^\gamma$  are given by [64]

$$\begin{aligned}
d_q^{\gamma h} &= \frac{e_q e^4}{64\pi^4 s_w m_W} \frac{\sqrt{x_q x_{\chi_i^+}}}{x_h} \Im [C_{\bar{\chi}_i^+ h \chi_i^+}^L] f_{\gamma H} \left( \frac{x_{\chi_i^+}}{x_h} \right), \\
d_q^{Z h} &= \frac{e^3 (T_{3q} - 2e_q s_w^2)}{(4\pi)^4 c_w s_w^2 m_W} \frac{\sqrt{x_q x_{\chi_i^+}}}{x_h} \Im [C_{\bar{\chi}_i^+ h \chi_j^+}^L C_{\bar{\chi}_j^+ h \chi_i^+}^L - C_{\bar{\chi}_i^+ h \chi_j^+}^R C_{\bar{\chi}_j^+ h \chi_i^+}^R] f_{ZH} \left( \frac{x_Z}{x_h}, \frac{x_{\chi_i^+}}{x_h}, \frac{x_{\chi_j^+}}{x_h} \right), \\
d_q^{WW} &= \frac{T_{3q} e^3}{128\pi^4 s_w^2 m_W} \sqrt{x_q x_{\chi_i^+} x_{\chi_j^0}} \Im [C_{\bar{\chi}_j^0 W_\mu^+ \chi_i^+}^R C_{\bar{\chi}_j^0 W_\mu^+ \chi_i^+}^{L*}] f_{WW} (x_{\chi_i^+}, x_{\chi_j^0}), \tag{21}
\end{aligned}$$

where  $s_w \equiv \sin \theta_W$ ,  $c_w \equiv \cos \theta_W$ , and  $\theta_W$  is the Weinberg angle,  $T_{3q}$  denotes the isospin of

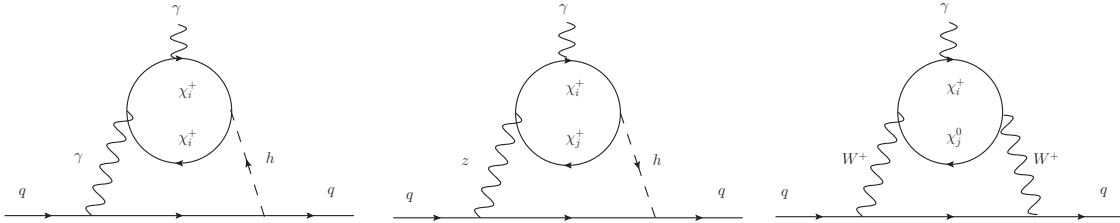


FIG. 4: The two-loop Barr-Zee type diagrams contributing to the quark EDM. The diagrams in which the photon or gluon is emitted from the  $W$  boson or the internal fermion do not contribute to the quark EDM or CEDM.

the corresponding quark, the functions  $f_{\gamma H}$ ,  $f_{ZH}$ ,  $f_{WW}$  can be found in Ref. [64].

#### IV. NUMERICAL ANALYSES

In this section, we present the numerical results of the EDMs  $d_n$ ,  $d_b$  and  $d_c$  in the B-LSSM. For SM parameters, we take  $m_W = 80.385$  GeV,  $m_Z = 90.1876$  GeV,  $m_u = 2.3$  MeV,  $m_d = 4.8$  MeV,  $m_b = 4.65$  GeV,  $m_c = 1.275$  GeV,  $\alpha_{em}(m_Z) = 1/128.9$ ,  $\alpha_s(m_Z) = 0.118$ . The SM-like Higgs boson mass is 125.09 GeV [65]. The updated experimental data [66] on searching  $Z'$  indicates  $M_{Z'} \geq 4.05$  TeV at 95% Confidence Level (CL). And Refs. [67, 68] give us an upper bound on the ratio between the  $Z'$  mass and its gauge coupling at 99% CL as  $M_{Z'}/g_B > 6$  TeV. In addition, the LHC experimental data also constrain  $\tan \beta' < 1.5$ . Since the contributions from heavy  $Z'$  are highly suppressed, we approximately fix  $M_{Z'} = 4.2$  TeV without losing generality. In addition, we take charged Higgs boson mass  $M_{H^\pm} = 1.5$  TeV approximately, which can satisfy the experimental data on  $\bar{B} \rightarrow X_s \gamma$ ,  $B_s^0 \rightarrow \mu^+ \mu^-$  [69]. All parameters fixed above affect the numerical results negligibly. For the squark sector, we take  $m_{\bar{q}} = m_{\tilde{u}} = m_{\tilde{d}} = \text{diag}(M_Q, M_Q, M_Q)$  TeV and  $T_{u,d} = \text{diag}(A_Q, A_Q, A_Q)$  TeV for simplicity. The observed Higgs signal limits that  $M_Q > 1.5$  [70].

Since the two-loop gluino corrections are included in our calculation,  $\theta_3$  which is the phase of gluino mass  $M_3$  can make contributions to  $d_n$ ,  $d_b$  and  $d_c$  through these two-loop gluino diagrams. In addition, the  $\mu$  term makes the dominate contributions to the EWB, and the corresponding CPV phase  $\theta_\mu$  is requested to be large. Meanwhile,  $\theta_\mu$  can make contributions

to these EDMs through both the two-loop gluino and Barr-Zee type diagrams. Hence, the effects of  $\theta_3$  and  $\theta_\mu$  to these EDMs are interesting. Then, considering the constraints from the experiments [10], we take  $M_1 = \frac{1}{2}M_2 = \frac{1}{2}M_{B'} = \frac{1}{2}M_{BB'} = \frac{1}{2}\mu = 0.3$  TeV,  $M_3 = 0.3$  TeV,  $\mu' = 0.8$  TeV,  $\tan\beta = 10$ ,  $\tan\beta' = 1.15$ ,  $g_B = 0.4$ ,  $g_{\nu B} = -0.4$ ,  $M_Q = 2$ ,  $A_Q = 0.1$ , all other CPV phases to be zero. Without specific illustrations, the parameters are taken as the above values. Then we plot  $d_n$  versus  $\theta_3$ ,  $\theta_\mu$  in Fig. 5(a), (b) respectively, where the solid, dashed and dotted lines denote the one-loop result, the sum of one-loop and two-loop gluino results, the sum of one-loop and two-loop Barr-Zee type results respectively. There is no dotted line in Fig. 5(a), because  $\theta_3$  do not make contributions through Barr-Zee type diagrams. Similarly,  $d_b$  versus  $\theta_3$ ,  $\theta_\mu$  are plotted in Fig. 5(c), (d), and  $d_c$  versus  $\theta_3$ ,  $\theta_\mu$  are plotted in Fig. 5(e), (f).

Fig. 5(a), (c) show that, when the only CPV contributions come from  $\theta_3$ , the relative contributions from two-loop gluino diagrams to one-loop contributions of  $d_n$ ,  $d_b$  can reach around 14%, 10% respectively, which produces more precise predictions on these quantities. From Fig. 5(e) we can see that, the two-loop gluino corrections make the dominate contributions to  $d_c$ , with respect to the one-loop corrections. It can be seen in Fig. 5(b), (d), (f) that, the two-loop gluino corrections can make more important contributions with lighter quark, and the two-loop gluino corrections to  $d_n$ ,  $d_c$  are even larger than the corresponding one-loop results. When the only CPV contributions come from  $\theta_\mu$ , the dominate contributions of one-loop and two-loop gluino corrections to quark EDMs come from charginos, and Yukawa coupling constant appears in the right-hand part of the interaction vertex chargino-quark-squark. Hence, the expression of  $d_q^{\gamma, g(3)}$  in Eq. (16) shows that, the contributions from charginos are proportional to Yukawa coupling constant. However, for the two-loop gluino corrections when charginos appear as internal particles, in Eq. (20), there is a term does not depend on Yukawa coupling constant, this is why the two-loop gluino diagrams can make dominate corrections to  $d_n$  or  $d_c$ . In addition, Eq. (21) shows that, the two-loop Barr-Zee type corrections are proportional to  $m_q/m_W$ , which can be seen directly by comparing the dotted lines in Fig. 5(b), (d), (f). It also can be noted that, the most strict constraints on  $\theta_3$  and  $\theta_\mu$  come from the experimental upper bound on  $d_n$ . And the contributions from  $\theta_3$  to  $d_n$  is larger than the contributions from  $\theta_\mu$ , hence the contributions from large  $\theta_\mu$ , which

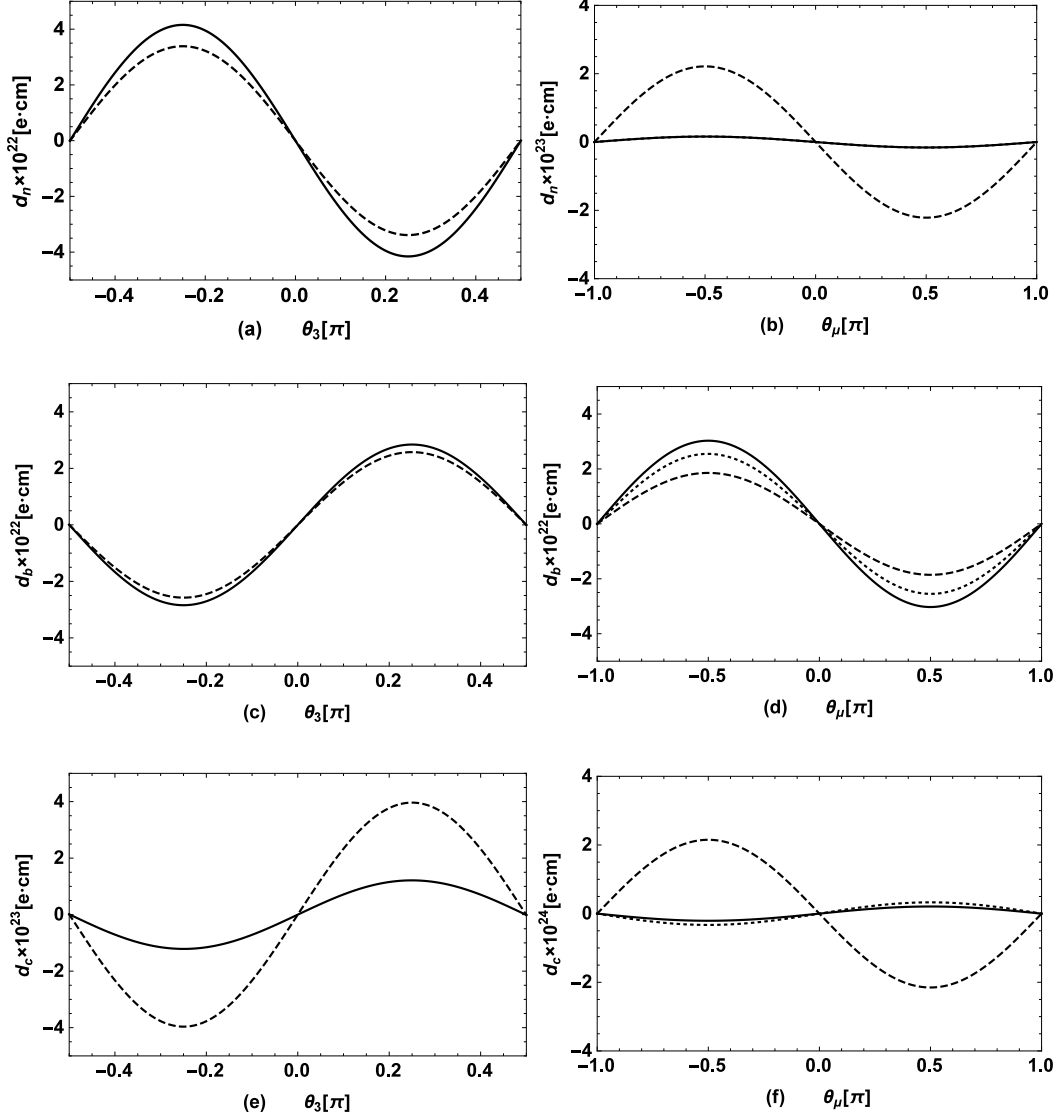


FIG. 5:  $d_n$ ,  $d_b$ ,  $d_c$  versus  $\theta_3$ ,  $\theta_\mu$  are plotted, where the solid, dashed and dotted lines denote the one loop results, the sum of one-loop and two-loop gluino results, the sum of one-loop and two-loop Barr-Zee type results respectively.

is needed to generate the baryon asymmetry, can be cancelled by appropriate  $\theta_3$ . From the picture we can also note that, the theoretical prediction of  $d_c$  is well below the present upper bound in our chosen parameter space, which indicates the present upper bound on  $d_c$  limits the parameter space of the B-LSSM weakly.

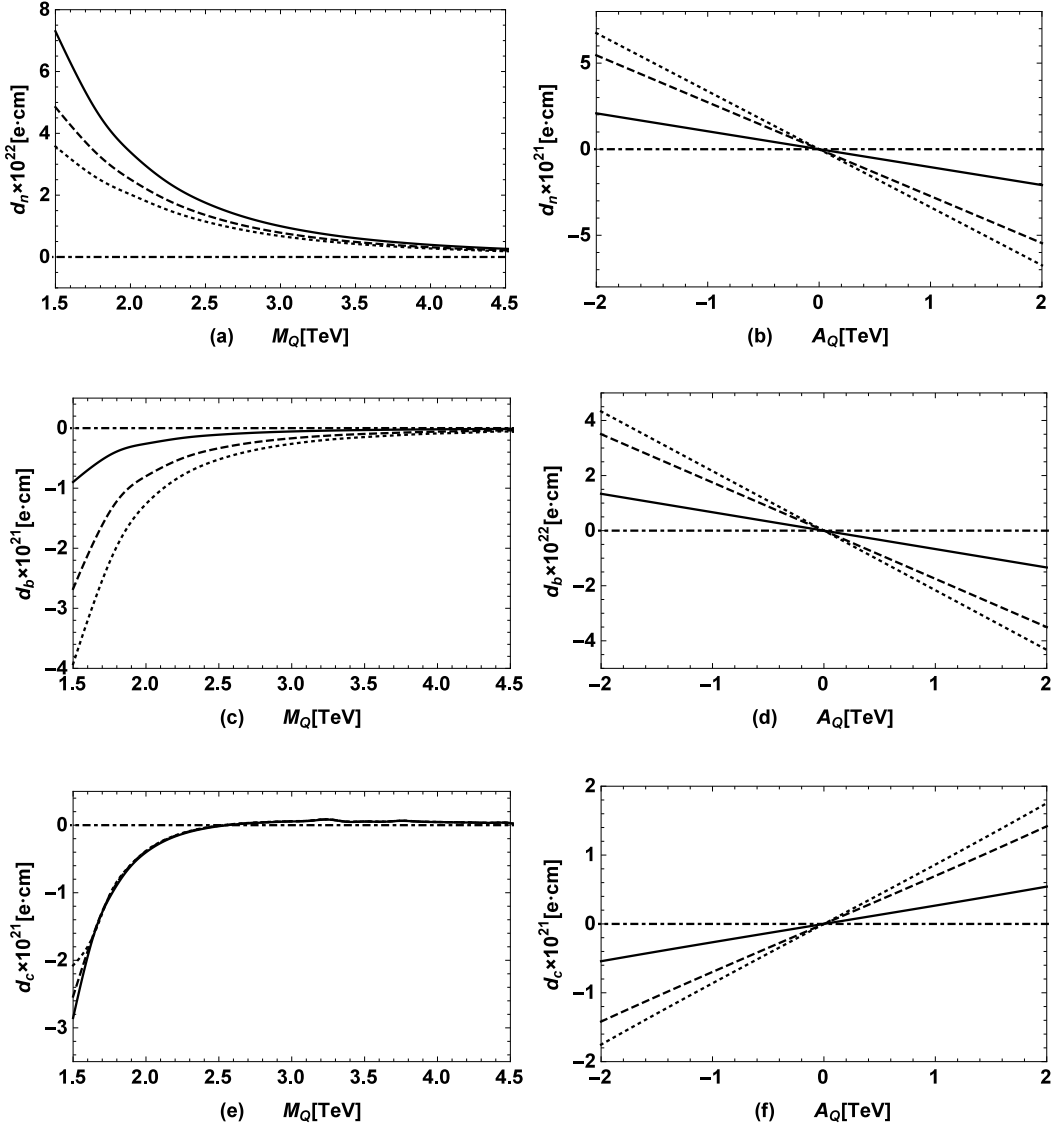


FIG. 6:  $d_n$ ,  $d_b$ ,  $d_c$  versus  $M_Q$  for  $\tan \beta = 10$  (solid line), 20 (dashed line), 30 (dotted line), and  $A_Q$  for  $\theta_A = 0.1$  (solid line), 0.3 (dashed line), 0.5 (dotted line) are plotted, where the dotdashed lines denote  $d_n = d_b = d_c = 0$ .

Since both the two-loop gluino and Barr-Zee type diagrams can make important contributions to the numerical results, we take the summing of all contributions from these two-loop and one-loop corrections in the following analysis. Then in order to see how  $M_Q$ ,  $\tan \beta$  affect the numerical results, taking  $\theta_3 = -0.25$  and other CPV phases to be zero,  $d_n$  versus  $M_Q$  for

$\tan\beta = 10$  (solid line), 20 (dashed line), 30 (dotted line) are plotted in Fig. 6(a). Similarly,  $d_b$  and  $d_c$  versus  $M_Q$  are plotted in Fig. 6(c), (e). In addition, the trilinear scalar terms  $T_{u,d}$  can also have CPV phase  $\theta_A$ , assuming  $\tan\beta = 10$ ,  $M_Q = 2$ , and all other phases are zero,  $d_n$  versus  $A_Q$  for  $\theta_A = 0.1$  (solid line), 0.3 (dashed line), 0.5 (dotted line) are plotted in Fig. 6(b). Similarly,  $d_b$  and  $d_c$  versus  $A_Q$  are plotted in Fig. 6(d), (f). In the picture, the dotdashed lines denote  $d_n = d_b = d_c = 0$ , which is plotted for analyzing the effects of  $M_Q$ ,  $\tan\beta$ ,  $A_Q$  and  $\theta_A$  conveniently.

Fig. 6(a), (c) show that, the contributions to  $d_n$ ,  $d_b$  decrease with the increasing of  $M_Q$ , which coincides with the decoupling theorem. However, the sign of  $d_c$  is changed when  $M_Q > 2.7$  TeV, and then  $d_c$  keeps going down to zero with the increasing of  $M_Q$ , which can be seen in Fig. 6(e). The dominate contributions to  $d_q$  come from  $d_q^\gamma$  when  $M_Q$  is small, and  $d_q^\gamma$  decreases more quickly than  $d_q^g$  with the increasing of  $M_Q$ . For  $c$  quark, the signs of  $d_c^\gamma$  and  $d_c^g$  are opposite, and the contributions from  $d_c^g$  are larger than  $d_c^\gamma$  as  $M_Q > 2.7$  TeV, hence  $d_c$  varying with  $M_Q$  as in Fig. 6(e). In addition, it obvious that  $\tan\beta$  can affect the numerical results of  $d_n$ ,  $d_b$  obviously, while  $\tan\beta$  affects  $d_c$  negligibly, and the effects of  $\tan\beta$  are suppressed when  $M_Q$  is large.  $\tan\beta$  affects the numerical results mainly through affecting the squark masses and the corresponding Yukawa coupling constants of quark. From Fig. 6(b), (d), (f) we can see that  $\theta_A$  can also make important contributions to these EDMs, and the effects of  $\theta_A$  can be enlarged by large  $|A_Q|$ . In addition, the signs of  $d_{n,b,c}$  can be changed when we take the sign of  $A_Q$  be opposite.

Comparing with the MSSM, there are two new mass terms  $M_{BB'}$  and  $M_{B'}$  in the B-LSSM, which can also have CPV phases  $\theta_{M_{BB'}}$ ,  $\theta_{M_{B'}}$  respectively. Both of  $M_{BB'}$  and  $M_{B'}$  can be very small and the gaugino masses are still large enough to satisfy the experimental lower bounds on gaugino masses. The contributions to these EDMs from the phases  $\theta_{M_{BB'}}$  or  $\theta_{M_{B'}}$  can be highly suppressed by small  $M_{BB'}$  or  $M_{B'}$  to satisfy the present experimental upper bounds on these EDMs. Assuming all contributions from other phases are cancelled each other completely, and the only contributions to these EDMs come from  $\theta_{M_{BB'}}$ ,  $\theta_{M_{B'}}$ , then  $d_n$  versus  $\theta_{M_{BB'}}$  are plotted in Fig. 7(a) for  $M_{BB'} = 0.3$  GeV (solid line),  $M_{BB'} = 0.6$  GeV (dashed line),  $M_{BB'} = 0.9$  GeV (dotted line), and  $d_n$  versus  $\theta_{M_{B'}}$  are plotted in Fig. 7(b) for  $M_{B'} = 10$  GeV (solid line),  $M_{B'} = 20$  GeV (dashed line),  $M_{B'} = 30$  GeV (dotted line),

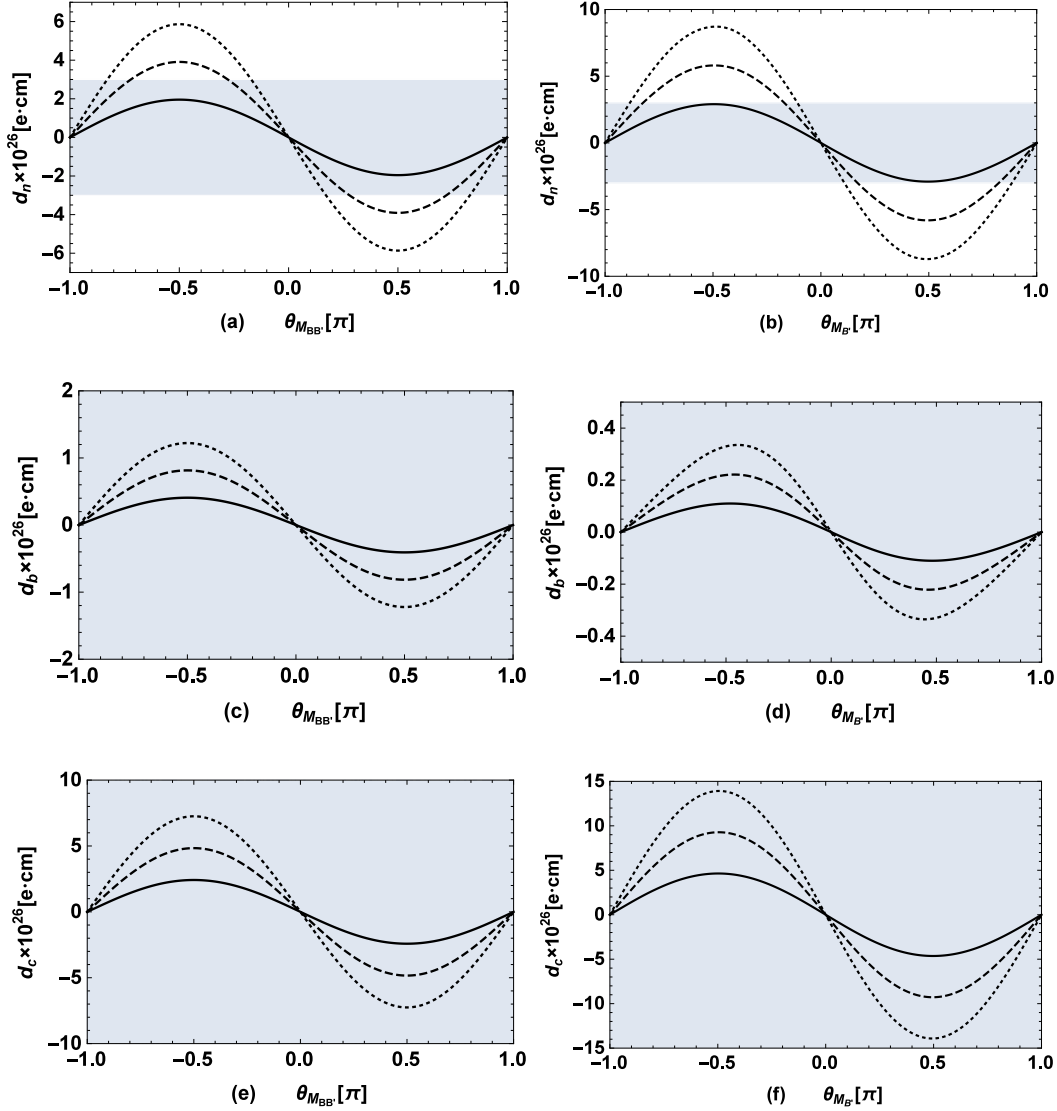


FIG. 7:  $d_n$ ,  $d_b$ ,  $d_c$  versus  $\theta_{M_{BB'}}$  for  $M_{BB'} = 0.3$  GeV (solid line),  $M_{BB'} = 0.6$  GeV (dashed line),  $M_{BB'} = 0.9$  GeV (dotted line), and  $\theta_{M_{B'}}$  for  $M_{B'} = 10$  GeV (solid line),  $M_{B'} = 20$  GeV (dashed line),  $M_{B'} = 30$  GeV (dotted line) are plotted, where the gray areas denote the allowed region below the present experimental upper bounds on  $d_n$ ,  $d_b$ ,  $d_c$  respectively.

where the gray areas denote the allowed region below the present experimental upper bound on  $d_n$ . Similarly, we plot  $d_b$  versus  $\theta_{M_{BB'}}$ ,  $\theta_{M_{B'}}$  in Fig. 7(c), (d), and  $d_c$  versus  $\theta_{M_{BB'}}$ ,  $\theta_{M_{B'}}$  in Fig. 7(e), (f) respectively.

parameters	min	max	step
$M_1[\text{TeV}]$	0.2	1	0.05
$M_2[\text{TeV}]$	0.2	1	0.05
$\mu[\text{TeV}]$	0.2	1.5	0.05

TABLE I: Scanning parameters for Fig. 8(a), (c), (e).

parameters	min	max	step
$\tan \beta'$	1.1	1.5	0.02
$g_B$	0.2	0.7	0.02
$g_{YB}$	-0.7	-0.2	0.02

TABLE II: Scanning parameters for Fig. 8(b), (d), (f).

Fig. 7(a), (b) show that, the present experimental upper bound on  $d_n$  limits  $M_{BB'} \lesssim 0.3$  GeV when the range of  $\theta_{M_{BB'}}$  is fully relaxed, while  $M_{B'} \lesssim 10$  GeV when the range of  $\theta_{M_{B'}}$  is fully relaxed. It can be noted that,  $M_{BB'}$  is limited more strictly than  $M_{B'}$ , because  $M_{BB'}$  is the mixing term between  $\tilde{\lambda}_B$  and  $\tilde{\lambda}_{B'}$ , it can contribute to these EDMs through the channel of  $\tilde{\lambda}_B$  and  $\tilde{\lambda}_{B'}$ , when  $M_{B'}$  contributes to these EDMs only through the channel of  $\tilde{\lambda}_{B'}$ . In addition, Fig. 7(c)-(f) show that, the theoretical predictions on  $d_b$ ,  $d_c$  are well below the present upper bounds correspondingly. And theoretical prediction on  $d_c$  is comparable with  $d_b$ , which is different from the case in Fig. 5(d), (f). The main difference between  $d_b$  and  $d_c$  is Yukawa coupling constants, and  $\theta_{M_{BB'}}$ ,  $\theta_{M_{B'}}$  affect the numerical results mainly through  $\tilde{\lambda}_B$ ,  $\tilde{\lambda}_{B'}$ , which are the super partners of gauge bosons corresponding to  $U(1)_Y$  and  $U(1)_{B-L}$ . Hence, theoretical prediction on  $d_b$  is not larger than  $d_c$  necessarily when the only contributions to them come from  $\theta_{M_{BB'}}$  or  $\theta_{M_{B'}}$ . In addition, it can be noted from the picture that, the effects of  $\theta_{M_{BB'}}$  or  $\theta_{M_{B'}}$  are enlarged by large  $M_{BB'}$  or  $M_{B'}$ , in our chosen parameter space.

In the neutralino sector,  $M_1$ ,  $M_2$  and  $\mu$  can also affect the numerical results. In order to see the effects of them, we take  $\theta_\mu = -0.5$ , and scan the parameter space shown in Table. I. Then  $d_n$  versus  $\mu$  are plotted in Fig. 8 (a). In addition, with respect to the MSSM, there are three new parameters  $\tan \beta'$ ,  $g_B$  and  $g_{YB}$  in the B-LSSM, which can also affect the theoretical

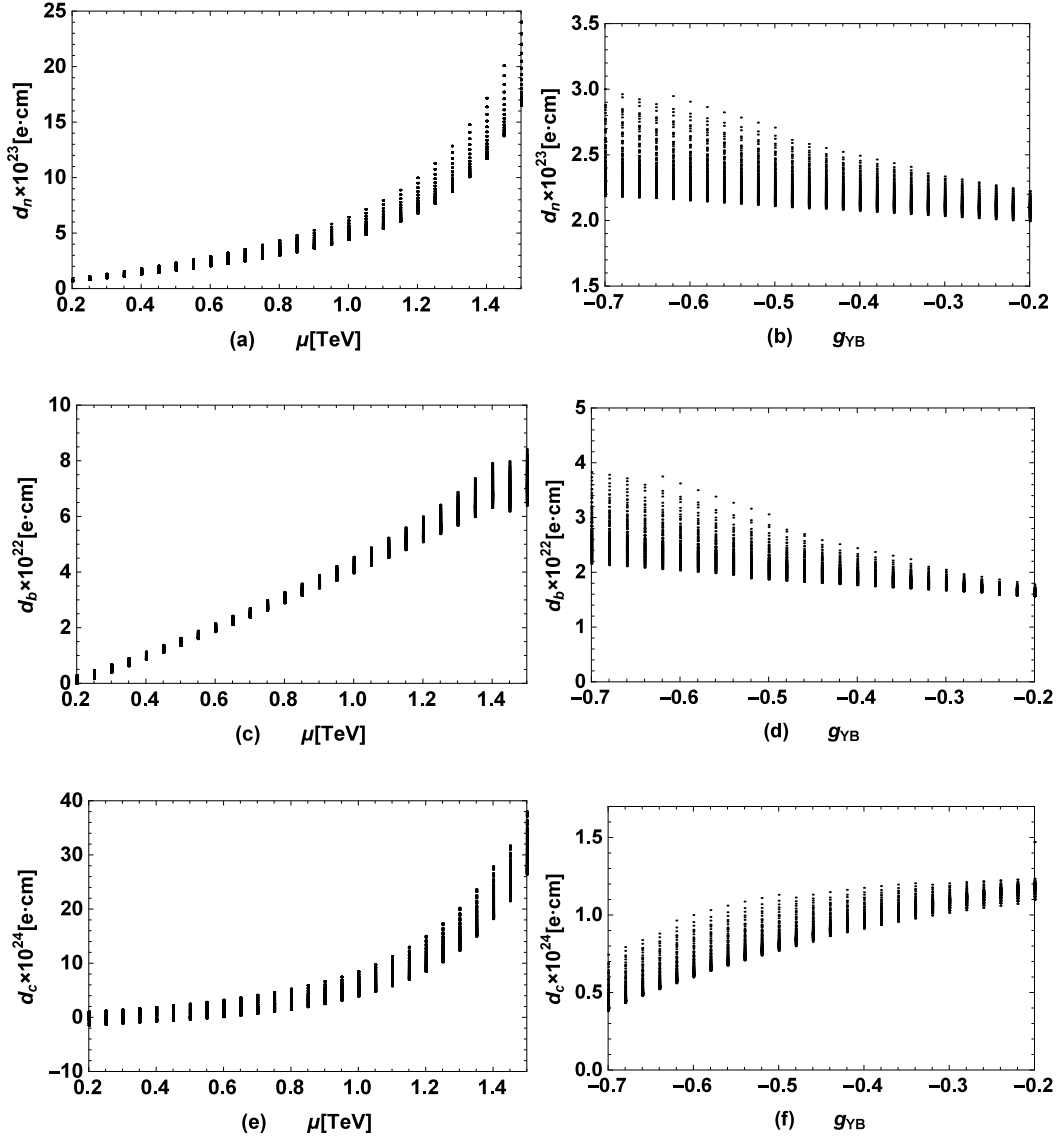


FIG. 8: Scanning the parameter space shown in Table. I, Table. II respectively,  $d_n$ ,  $d_b$  and  $d_c$  versus  $\mu$ ,  $\tan \beta'$  are plotted.

predictions on  $d_{n,b,c}$ . We scan the parameter space shown in Table. II. Since  $\tan \beta'$ ,  $g_B$ ,  $g_{YB}$  can affect the squark masses and the SM-like Higgs boson mass, we keep the squark masses  $M_{\tilde{U}_a, \tilde{D}_a} > 1.5$  TeV ( $a = 1, \dots, 6$ ), the SM-like Higgs boson mass in experimental  $3\sigma$  interval  $125.09 \pm 0.72$  GeV in the scanning, to avoid the range ruled out by the experiments. Then we plot  $d_n$  versus  $g_{YB}$  in Fig. 8 (b). Similarly,  $d_b$ ,  $d_c$  versus  $\mu$  are plotted in Fig. 8 (c), (e),

and  $d_b$ ,  $d_c$  versus  $g_{YB}$  are plotted in Fig. 8 (d), (f) respectively.

Fig. 8 (a), (c), (e) show that,  $d_n$ ,  $d_b$ ,  $d_c$  increase with the increasing of  $\mu$ , and  $\mu$  affects the numerical results more obviously than  $M_1$ ,  $M_2$ , because the only CPV source in our chosen parameter space is  $\theta_\mu$ , and the effects of  $\theta_\mu$  can be enlarged by large  $\mu$ . In addition,  $M_1$ ,  $M_2$  mix with  $\mu$  in the mass matrix of neutralino at the tree level, hence  $\theta_\mu$  can make contributions to these EDMs through the channel of  $M_1$ ,  $M_2$ , and  $M_1$ ,  $M_2$  affect the numerical results more obviously when  $\mu$  is larger, which can be noted in Fig. 8 (a), (c), (e). Fig. 8 (b), (d), (f) show that,  $d_n$ ,  $d_b$  decrease slowly with the decreasing of  $|g_{YB}|$ , while  $d_c$  increases with the decreasing of  $|g_{YB}|$ , and the effects of  $\tan\beta'$ ,  $g_B$ ,  $g_{YB}$  on the numerical results are comparable in our chosen parameter space.  $\tan\beta'$ ,  $g_B$ ,  $g_{YB}$  affect the numerical results mainly by affecting the squark masses and the mixing in the neutralino sector.

## V. SUMMARY

In this work, we explore the EDMs of neutron  $d_n$  and heavy quarks  $d_b$ ,  $d_c$  in the B-LSSM. In the calculation, some two loop gluino and Barr-Zee type diagrams are considered. With respect to the MSSM, there are new CPV phases of two additional mass terms in the neutralino sector, which can make contributions to these EDMs through both one-loop and two-loop corrections. And new parameters  $\tan\beta'$ ,  $g_B$ ,  $g_{YB}$  in the B-LSSM can also affect the numerical results by affecting the squark masses and the mixing in the neutralino sector. Considering the constraints from updated experimental data, the numerical results show that, the two-loop gluino diagrams can make important corrections to  $d_{n,b,c}$ , while the two-loop Barr-Zee type diagrams can make important corrections to  $d_{b,c}$ . The most strict constraints on  $\theta_3$  and  $\theta_\mu$  come from the experimental upper bound on  $d_n$ , and the contributions from large  $\theta_\mu$ , which is needed for the taking place of EWB, can be cancelled by the contributions from  $\theta_3$ . In addition, when the contributions to  $d_{n,b,c}$  from CPV phases in the MSSM are cancelled each other completely, new phase parameters  $\theta_{MBB'}$ ,  $\theta_{MB'}$  in the B-LSSM also can make contributions to these quantities. And with respect to the MSSM, new parameters  $\tan\beta'$ ,  $g_B$ ,  $g_{YB}$  in the B-LSSM affect the theoretical predictions on  $d_{n,b,c}$  comparably.

## Acknowledgments

The work has been supported by the National Natural Science Foundation of China (NNSFC) with Grants No. 11535002, No. 11647120, and No. 11705045, Natural Science Foundation of Hebei province with Grants No. A2016201010 and No. A2016201069, the youth top-notch talent support program of the Hebei Province, Hebei Key Lab of Optic-Eletronic Information and Materials, and the Midwest Universities Comprehensive Strength Promotion project.

- 
- [1] J. H. Christenson, J. W. Cronin, V. L. Fitch and R. Turlay, Phys. Rev. Lett. **13**, 138 (1964).
  - [2] K. Abe *et al.* [Belle Collaboration], Phys. Rev. Lett. **87**, 091802 (2001).
  - [3] B. Aubert *et al.* [BaBar Collaboration], Phys. Rev. Lett. **89**, 201802 (2002).
  - [4] J. R. Ellis, S. Ferrara and D. V. Nanopoulos, Phys. Lett. **114B**, 231 (1982).
  - [5] J. Polchinski and M. B. Wise, Phys. Lett. **125B**, 393 (1983).
  - [6] P. Nath, Phys. Rev. Lett. **66**, 2565 (1991).
  - [7] Y. Kizukuri and N. Oshimo, Phys. Rev. D **46**, 3025 (1992).
  - [8] Y. Kizukuri and N. Oshimo, Phys. Rev. D **45**, 1806 (1992).
  - [9] J. Baron et al, (ACME Collaboration), Science **343**, 269 (2014).
  - [10] M. Tanabashi et al, (Particle Data Group), Phys. Rev. D **98**, 030001 (2018).
  - [11] V. Andreev et al, (ACME Collaboration), Nature **562**, 355-360 (2018).
  - [12] A. E. Blinov and A. S. Rudenko, Nucl. Phys. Proc. Suppl. **189**, 257 (2009).
  - [13] F. Sala, JHEP **1403**, 061 (2014).
  - [14] M. Pospelov and A. Ritz, Phys. Rev. D **63**, 073015 (2001).
  - [15] E. Braaten, C. S. Li and T. C. Yuan, Phys. Rev. Lett. **64**, 1709 (1990).
  - [16] G. Degrassi, E. Franco, S. Marchetti and L. Silvestrini, JHEP **0511**, 044 (2005).
  - [17] H. Gisbert and J. Ruiz Vidal, arXiv:1905.02513 [hep-ph].
  - [18] D. Chang, W. Y. Keung, C. S. Li and T. C. Yuan, Phys. Lett. B **241**, 589 (1990).
  - [19] M. Dine, P. Huet, R. L. Singleton, Jr and L. Susskind, Phys. Lett. B **257**, 351 (1991).

- [20] A. G. Cohen and A. E. Nelson, Phys. Lett. B **297**, 111 (1992) [hep-ph/9209245].
- [21] P. Huet and A. E. Nelson, Phys. Rev. D **53**, 4578 (1996).
- [22] C. Lee, V. Cirigliano and M. J. Ramsey-Musolf, Phys. Rev. D **71**, 075010 (2005).
- [23] T. Konstandin, T. Prokopec, M. G. Schmidt and M. Seco, Nucl. Phys. B **738**, 1 (2006) [hep-ph/0505103].
- [24] T. Falk and K. A. Olive, Phys. Lett. B **375**, 196 (1996).
- [25] T. Falk and K. A. Olive, Phys. Lett. B **439**, 71 (1998).
- [26] M. Brhlik, G. J. Good and G. L. Kane, Phys. Rev. D **59**, 115004 (1999).
- [27] A. Bartl, T. Gajdosik, W. Porod, P. Stockinger and H. Stremnitzer, Phys. Rev. D **60**, 073003 (1999).
- [28] S. Abel, S. Khalil and O. Lebedev, Nucl. Phys. B **606**, 151 (2001) [hep-ph/0103320].
- [29] V. D. Barger, T. Falk, T. Han, J. Jiang, T. Li and T. Plehn, Phys. Rev. D **64**, 056007 (2001) [hep-ph/0101106].
- [30] K. A. Olive, M. Pospelov, A. Ritz and Y. Santoso, Phys. Rev. D **72**, 075001 (2005) [hep-ph/0506106].
- [31] V. Cirigliano, S. Profumo and M. J. Ramsey-Musolf, JHEP **0607**, 002 (2006) [hep-ph/0603246].
- [32] S. Y. Ayazi and Y. Farzan, Phys. Rev. D **74**, 055008 (2006)
- [33] V. Barger, P. Fileviez Perez and S. Spinner, Phys. Rev. Lett **102**, 181802 (2009) [arXiv:0812.3661 [hep-ph]].
- [34] P. Fileviez Perez and S. Spinner, Phys. Lett. B **673**, 251 (2009) [arXiv:0811.3424 [hep-ph]].
- [35] M. Ambroso and B. A. Ovrut, Int. J. Mod. Phys. A **26**, 1569 (2011) [arXiv:1005.5392 [hep-th]].
- [36] P. F. Perez and S. Spinner, Phys. Rev. D **83**, 035004 (2011).
- [37] S. Khalil and H. Okada, Phys. Rev. D **79**, 083510 (2009) [arXiv:0810.4573 [hep-ph]].
- [38] L. Basso, B. OLeary, W. Porod and F. Staub, JHEP **1209**, 054 (2012) [arXiv:1207.0507 [hep-ph]].
- [39] L. Delle Rose, S. Khalil, S. J. D. King, C. Marzo, S. Moretti and C. S. Un, Phys. Rev. D **96**, 055004 (2017) [arXiv:1702.01808 [hep-ph]].
- [40] L. Delle Rose, S. Khalil, S. J. D. King, S. Kulkarni, C. Marzo, S. Moretti and C. S. Un, JHEP

- 1807**, 100 (2018) [arXiv:1712.05232 [hep-ph]].
- [41] A. Elsayed, S. Khalil and S. Moretti, Phys. Lett. B **715**, 208 (2012) [arXiv:1106.2130 [hep-ph]].
- [42] G. Brooijmans et al. [arXiv:1203.1488 [hep-ph]].
- [43] L. Basso and F. Staub, Phys. Rev. D **87**, 015011 (2013) [arXiv:1210.7946 [hep-ph]].
- [44] L. Basso et al., Comput. Phys. Commun. **184**, 698 (2013) [arXiv:1206.4563 [hep-ph]].
- [45] A. Elsayed, S. Khalil, S. Moretti and A. Moursy, Phys. Rev. D **87**, 053010 (2013) [arXiv:1211.0644[hep-ph]] .
- [46] S. Khalil and S. Moretti, Rept. Prog. Phys **80**, 036201 (2017) [arXiv:1503.08162 [hep-ph]].
- [47] W. Abdallah, A. Hammad, S. Khalil and S. Moretti, Phys. Rev. D **95**, 055019 (2017) [arXiv:1608.07500 [hep-ph]].
- [48] C. S. Aulakh, A. Melfo, A. Rasin and G. Senjanovic, Phys. Lett. B **459**, 557 (1999) [hep-ph/9902409].
- [49] F. Staub, arXiv:0806.0538. F. Staub, Comput. Phys. Commun. **181** 1077-1086 (2010) [arXiv:0909.2863]. F. Staub, Comput. Phys. Commun. **182** 808-833 (2011) [arXiv:1002.0840]. F. Staub, Comput. Phys. Commun. **184** 1792-1809 (2013) [arXiv:1207.0906]. F. Staub, Comput. Phys. Commun. **185** 1773-1790 (2014) [arXiv:1309.7223].
- [50] B. Holdom, Phys. Lett. B **166**, 196 (1986).
- [51] T. Matsuoka and D. Suematsu, Prog. Theor. Phys. **76**, 901 (1986).
- [52] F. del Aguila, G. D. Coughlan and M. Quiros, Nucl. Phys. B **307**, 633 (1988).
- [53] F. del Aguila, J. A. Gonzalez and M. Quiros, Nucl. Phys. B **307**, 571 (1988).
- [54] F. del Aguila, G. D. Coughlan and M. Quiros, Nucl. Phys. B **312**, 751 (1988).
- [55] R. Foot and X. G. He, Phys. Lett. B **267**, 509 (1991).
- [56] K. S. Babu, C. F. Kolda and J. March-Russell, Phys. Rev. D **57**, 6788 (1998) [hep-ph/9710441].
- [57] J. L. Yang, T. F. Feng, H. B. Zhang, G. Z. Ning and X. Y. Yang, Eur. Phys. J. C **78**, 438 (2018).
- [58] J. L. Yang, T. F. Feng, Y. L. Yan, W. Li, S. M. Zhao and H. B. Zhang, Phys. Rev. D **99**, 015002 (2019).
- [59] J. Dai, H. Dykstra, R. G. Leigh, S. Paban and D. Dicus, Phys. Lett. B **237**, 216 (1990) Erratum: [Phys. Lett. B **242**, 547 (1990)].

- [60] D. A. Dicus, Phys. Rev. D **41**, 999 (1990).
- [61] T. Ibrahim and P. Nath, Phys. Rev. D **58**, 111301(R) (1998) Erratum: [Phys. Rev. D **60**, 099902(E) (1999)].
- [62] R. L. Arnowitt, J. L. Lopez and D. V. Nanopoulos, Phys. Rev. D **42**, 2423 (1990).
- [63] T. F. Feng, X. Q. Li, J. Maalampi and X. M. Zhang, Phys. Rev. D **71**, 056005 (2005).
- [64] G. F. Giudice and A. Romanino, Phys. Lett. B **634**, 307 (2006).
- [65] G. Aad *et al.* [ATLAS and CMS Collaborations], Phys. Rev. Lett **114**, 191803 (2015) [arXiv:1503.07589 [hep-ex]].
- [66] ATLAS Collab., ATLAS-CONF-2016-045.
- [67] G. Cacciapaglia, C. Csaki, G. Marandella, and A. Strumia, Phys.Rev. D **74**, 033011 (2006) [hep-ph/0604111] .
- [68] M. Carena, A. Daleo, B. A. Dobrescu and T. M. P. Tait, Phys. Rev. D **70**, 093009 (2004) [hep-ph/0408098] .
- [69] J. L. Yang, T. F. Feng, S. M. Zhao, R. F. Zhu, X. Y. Yang and H. B. Zhang, Eur. Phys. J. C **78**, 714 (2018).
- [70] C. S. Un and O. Ozdal, Phys. Rev. D **93**, 055024 (2016).